Optimization of fringe pattern calculation with direct correlations in speckle interferometry

Douglas R. Schmitt and R. W. Hunt

A direct correlation technique is used to calculate correlation fringe patterns from consecutive speckle patterns acquired with a dual-beam electronic speckle interferometer. Although more calculations are required than in standard image differencing routines, an advantage of the method is that the illumination over the surface of the object need not be uniform. In the method, Pearson's coefficient of correlation between the intensities within a set of adjacent pixels is calculated. This has the added advantage of being directly related to the theoretical phase-dependent correlation. A mapping of this measure of correlation results in the correlation fringe pattern. Laboratory tests were carried out with in-plane translations ranging from 5 to 45 μm. The correlation calculations were carried out by using cells (square sets of pixels) in the raw speckle images with dimensions ranging from 2 pixels × 2 pixels to 19 pixels × 19 pixels. Both cell dimension and translation magnitude dependent decorrelation effects influence the quality of the correlation fringe patterns. © 1997 Optical Society of America

1. Introduction

Since its invention in the early 1970's,[1] speckle correlation interferometry has shown much promise in the determination of three-dimensional micrometer-scale displacements and surface contours. The method employs the random pattern of dark and light spots, commonly referred to as speckles, observed on the surface of an optically rough surface illuminated by coherent light. This pattern results from the interference of light scattered randomly from the surface and has the remarkable quality that each individual speckle serves as a reference point from which changes in the phase of the light scattered from the surface can be tracked.[2–4] A great advantage is that the method requires only that the object under study be appropriately illuminated. Sample preparation is simplified, and the opportunities for disruptions of the object's behavior caused by the measurement method itself are minimized. As a result, speckle correlation interferometry has been applied in deformation analyses in a wide variety of disciplines, focusing mostly on engineering applications but also in medicine and botany. However, the varied geometries in which some such measurements must be carried out often do not allow workers to optimize optical systems for existing methods of speckle correlation. In particular, maintaining uniform illumination over large variably reflective objects can influence the quality of the conventional fringe patterns. Although the greatest challenges at present in speckle interferometry focus on issues relating fringe patterns to phase mappings, allowing the direct determination of displacements or strain, there is always room for complementary methodologies of determining the local correlation. In this paper we describe and test one such alternative method of calculating fringe patterns in speckle correlation interferometry.

In speckle pattern correlation interferometry the object is often illuminated with two coherent beams, both with spatially randomly varying intensities I_1 and I_2 and phases Ψ_1 and Ψ_2, the wave fields of which when combined in the image plane produce an initial image plane intensity

$$I_1 = I_1 + I_2 + 2\sqrt{I_1 I_2}\cos(\Psi_1 - \Psi_2) \qquad (1a)$$

and a postmotion intensity

$$I_2 = I_1 + I_2 + 2\sqrt{I_1 I_2}\cos(\Psi_1 - \Psi_2 + \Delta\phi), \qquad (1b)$$

where $\Delta\phi$ is the phase change in the light resulting from the displacement.[3]

The quality of the correlation between two speckle

The authors are with the Department of Physics, Institute of Geophysics, Meteorology, and Space Physics, University of Alberta, Edmonton, Alberta, Canada T6G 2J1.

Received 6 November 1996; revised manuscript received 27 January 1997.

0003-6935/97/348848-10$10.00/0

patterns acquired before and after deformation of an object is the basic quantity providing a measure of changes in phase of the light scattered from the surface. The intensity of each speckle varies cyclically in relation to the change in the phase as the surface of the object moves.[5] If the change in phase $\Delta\phi = 2n\pi$ (in-phase condition) then the speckle's intensity remains unchanged. In contrast, if the change in phase $\Delta\phi = (2n + 1)\pi$ (out-of-phase condition), then the intensity will differ randomly. As a result[1,5] a good correlation of speckle intensities is observed from regions of the displaced surface that are in phase, whereas there is no correlation when the out-of-phase condition exists. Further, the correlation coefficient ρ given by[6]

$$\rho = \frac{\langle I_1 I_2\rangle - \langle I_1\rangle\langle I_2\rangle}{(\langle I_1^2\rangle - \langle I_1\rangle^2)^{1/2}(\langle I_2^2\rangle - \langle I_2\rangle^2)^{1/2}} \tag{2}$$

has been shown to depend cylically on the change in the phase $\Delta\phi$ according to the simple relationship

$$\rho = \tfrac{1}{2}[1 + \cos(\Delta\phi)]. \tag{3}$$

The correlation coefficient ρ ranges according to a cosine relationship from 1 to 0 as $\Delta\phi$ evolves from in phase to out of phase. A mapping of this correlation over the surface of the object is reminiscent of a series of dark and bright fringes. This artificial fringe pattern contains information on the displacements of the object's surface. Unfortunately, the absolute value of the phase change $\Delta\phi$ is usually not known without additional constraints. The change in the phase at a given point on the surface of the object for the dual-beam experimental configuration described below is given by[7]

$$\Delta\phi = \frac{2\pi}{\lambda}(\mathbf{k}_1 - \mathbf{k}_2)\cdot\mathbf{d}, \tag{4}$$

where $\mathbf{k}_1$ and $\mathbf{k}_2$ are unit vectors describing the directions of the rays from the laser source points S_1 and S_2, respectively, to the point that experiences a displacement vector $\mathbf{d}$ between acquisition of the two speckle patterns.

A crucial aspect of the method is the determination of the correlation. Traditional photographic methods have been reviewed by Ennos[5] and include the photographic mask viewing of live fringes,[1] photographic subtraction,[1] exploitation of the nonlinearity inherent in photographic emulsions,[8] or use of the diffraction properties of the recorded speckle pattern itself.[5] Film-based methods are problematic owing to difficulties in the processing and final placement of the film sheets. However, as speckle correlation interferometry requires only that the speckles be independently resolvable, the use of video methods in recording and correlating the speckle patterns was recognized early[9–11] and because of its versatility has in recent years supplanted many of the film-based methods.[12–16] The video-based method is referred to as electronic speckle interferometry (ESPI).

A simple measure of the correlation between two

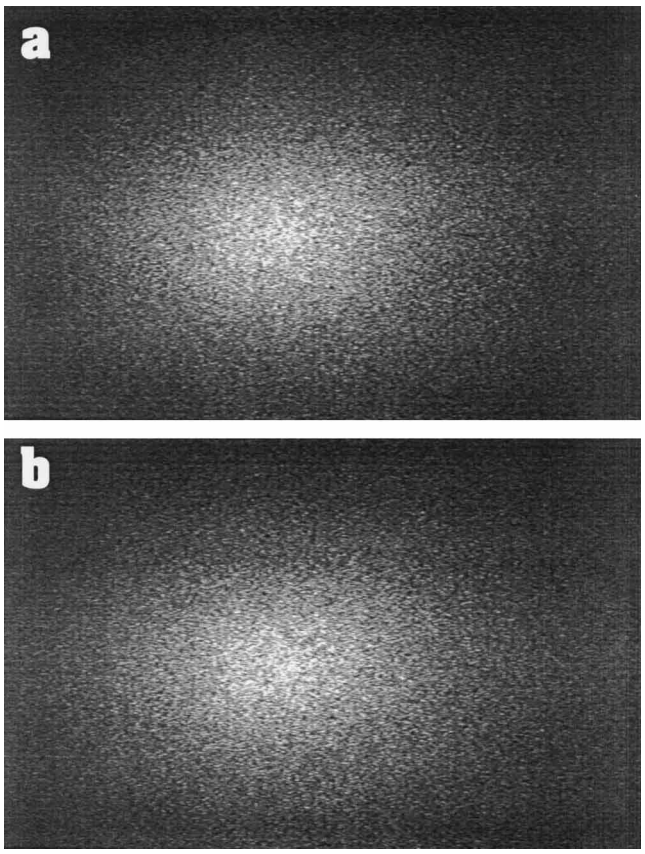

Fig. 1. Raw speckle patterns acquired, a, before and, b, after a 30-μm translation. Images include 756 horizontal × 486 vertical pixels and cover a range of 6.8 cm × 9.1 cm on the plate.

video images in ESPI is traditionally accomplished by rectifying or squaring the pixel-by-pixel voltage difference between subsequent patterns. In regions where the two speckle patterns correlate well the speckle intensities have nearly the same value, and as a result their subtraction produces values near zero, which may be displayed as a dark region in the final video image. Conversely, in out-of-phase regions with poor correlation the speckle intensity values differ and on average will be nonzero and will appear bright. Jones and Wykes[3] have also shown that the brightness within this subtraction image squared will be modulated by $\sin^2(\Delta\phi/2)$, the mapping of which also resembles a fringe pattern. This simple differencing procedure is particularly suited to the analysis of analog video signals. Calculation of this difference is computationally rapid, and as a result the differencing method survives in nearly all recent digital processing of speckle patterns.[16] Two raw speckle patterns of a flat surface acquired before and after a 30-μm translation are shown in Fig. 1 followed by their corresponding fringe patterns formed first by a simple pixel-by-pixel differencing and rectification (Fig. 2a) and second by pixel averaging before frame subtraction, rectification, and taking of the square root (Fig. 2b).

Such rectified difference mappings are also modulated, however, by the $\sin^2(\Psi_1 - \Psi_2 + \Delta\phi/2)$ term,

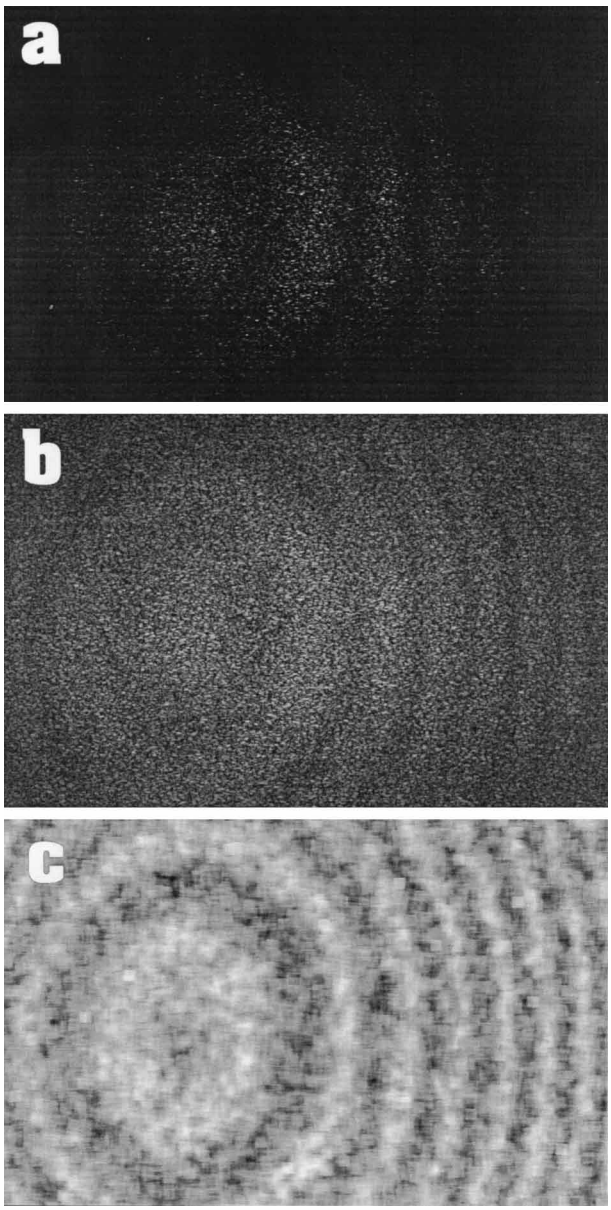

Fig. 2. Fringe patterns obtained from the raw frames of Fig. 1 by, a, squaring the pixel-by-pixel difference; b, pixel averaging then frame subtraction, rectification, and taking of the square root; c, direct correlation.

where $\Psi_1 - \Psi_2$ is the original phase from the speckle that appears as the high frequency and apparently random pixel-by-pixel intensity variation as seen in Fig. 1a. In digital form this reduces the levels of intensity available to fringe contrast; and the fringes appear more as changes in texture within the pattern. The fringe patterns are also sensitive to variations in the original illumination intensity over the surface of the object arising from the remnant $\sqrt{I_1 I_2}$ term in Eq. (1), and care must be taken to equalize this as much as possible. An example of poor illumination conditions produced by two divergent source beams on the surface of a plate is shown in Fig. 1. The corresponding mappings of the fringe pattern produced by the subtraction routines shown in Figs. 2a and 2b are of admitted low quality. Fringes are not clearly visible around the edges of Fig. 2a, where the light intensities in the original images of Fig. 1 were low; these fringes are more distinct in the pattern derived from pixel averaging, but the quality is still not comparable with that obtained with good illumination conditions. With brighter laser illumination, high intensities in the center of the plate were observed such that the CCD video detector was near saturation. As a result, the intensities in the two images did not differ substantially, and poor frame subtraction fringes result. The desired information containing $\sin^2(\Delta\phi/2)$ fringe term may, for example, be enhanced by appropriate bandpass filtering to remove the low-frequency background effects due to variable illumination across the surface and the high frequency $\sin^2(\Psi_1 - \Psi_2 + \Delta\phi/2)$ noise.[17] However, care must be exercised in this filtering to account for the influence of saturated regions, edges, and aliasing of the speckle noise into low-frequency components that could overlap the important fringe information.

In this paper we describe an alternative method of directly correlating digitally acquired speckle patterns; an application of this method with the same data is shown in Fig. 2c. This method requires more time-consuming calculations than the standard differencing technique but has the advantage that substantial fringe contrast is produced independent of the variations of illumination intensity over the surface of the object. For example, in Fig. 2c well-defined correlation fringes are observed over the entire image despite the nonuniform illumination. The immediate high-contrast fringes may not need additional processing in some applications. Further, the method described calculates the local discrete coefficient of correlation, which is directly related to the theoretical expression of Eq. (2). The paper first describes the methodology and then presents the results of laboratory micrometer-scale translational tests.

2. Analysis Methodology

The method directly relies on the result of Eqs. (2) and (3) that the correlation coefficient between two speckle patterns is modulated with a cosine dependence on the change in the phase $\Delta\phi$ experienced as a result of displacement. Consider two individual and complete speckle patterns digitally recorded before and after motion of the object with pixel intensities represented by A_{ij} and B_{ij}, respectively, where the indices i and j represent individual pixel positions within the images and each pixel represents on average the intensity of a single speckle. Further, assume temporarily that the displacements are sufficiently small, that speckle decorrelation effects[18] can be ignored, and that over suitably small spatially corresponding sets of m adjacent pixels a_k and b_k, referred to hereafter as cells, the change in the phase $\Delta\phi$ is nearly constant. The discrete local correlation coefficient r between these two cells and analogous to

the theoretical expression of Eq. (2) may be given explicitly by

$$r = \frac{\frac{1}{m}\sum^{m}(a_{k1}b_{k1}) - \left[\frac{1}{m}\sum^{m}(a_{k1})\right]\left[\frac{1}{m}\sum^{m}(b_{k1})\right]}{\sigma_a\sigma_b}, \quad (5)$$

where

$$\sigma_a = \left\{\frac{1}{m}\sum^{m}(a_{k1}{}^2) - \left[\frac{1}{m}\sum^{m}(a_{k1})\right]^2\right\}^{1/2} \quad (6)$$

with a corresponding formula for σ_b. This is the well-known Pearson's coefficient of correlation for finite discrete sets of data and is here taken to be an local approximation to the coefficient of correlation in Eq. (2). Note that Eq. (5) can produce only values between -1 and 1, and in this context only those between 0 and 1 have any meaning. This is a second advantage to the direct correlation method; use of r in place of ρ in Eq. (3) immediately yields the unwrapped value of the change in the phase $\Delta\phi$. Peng *et al.*[19] have attempted to use Eq. (5) applied over large areas of a speckle interferogram as a measure of the decorrelation effect. Most recently, Zhu and Chang[20] applied Eq. (5) to the correlation of objective speckles formed from simple illumination with a single beam to detect nodal points on the surface of a vibrating object.

Square cells are used in the present analysis. Once a cell size has been selected, the calculation of Eq. (5) is carried out systematically over each possible set of cells. The mapping of these calculated r values then forms the fringe pattern such as shown in Fig. 2c.

Equation (5) describes the quality of a linear regression fit between the pixel amplitudes in two corresponding speckle pattern cells. As suggested in Eq. (5), when the in-phase condition exists, r approaches unity, indicating good positive correlation. For the out-of-phase condition, r approaches zero, indicating no correlation. It is important to note that r values less than zero are possible with Eq. (5) but should not exist according to Eq. (3). Such values represent a negative correlation between the pixel intensitites within the two cells. Weakly negative values are encountered in practice because of the inherent random nature of the speckle intensities, but in the present context a negative correlation has the same meaning as no correlation and is assigned a value of zero. This has much the same effect as squaring in the standard subtraction method. If the same intensity level mapping is used, the sequence of dark and bright fringes calculated using Eq. (5) is exactly the opposite of that produced by the subtraction method, as may be observed in comparison of Fig. 2a and 2b with Fig. 2c. It is important to note that the direct correlation method does not provide any additional information over what is available in a high-quality fringe pattern formed by the more familiar and established frame subtraction. It is difficult to provide a quantitiative measure of the goodness of the fringe patterns in Fig. 2; however, it is likely that since the fringes are readily apparent in Fig. 2c that less processing might be necessary to extract the important phase information.

An advantage of using Eq. (5) is its greater independence from the local average illumination intensity, which is, for example, deleterious to the image contrast observed in Fig. 2a. This result again stems from the fact that Eq. (5) measures the quality of the correlation and does not depend on the local absolute value of the intensities unless these are so large or so small that the useful signal is either saturated or not detected. This even applies to potential temporal changes in the illumination intensity, which might result, for example, from fluctuations in the laser power from the initial to the second image. The result is clearly apparent in Fig. 2c, where high-contrast fringes calculated with the same two speckle images of Fig. 1 are observed over the entire mapping.

Application of Eq. (5) can rarely be carried out under the conditions stated above. First, the cell sizes must be finite; $\Delta\phi$ and consequently r cannot remain constant over the area of the cell such that there is some averaging of the response. This results in a loss of contrast in the mapped fringe pattern. Second, decorrelation effects[18] due to changes in the speckle pattern resulting from large displacements may also be important.

The primary factors influencing the quality of a calculated correlation fringe pattern include the dimensions of the correlation cell, the degree of decorrelation experienced as a result of motion, and the correlation fringe density within the final image. These are not unrelated to one another, and the analysis below attempts to quantify the effects of cell size and displacement magnitude in the final correlation fringe patterns.

The quality of a correlation fringe pattern is difficult to quantify. Hypothetically the correlation amplitudes within a perfect noise-free correlation fringe pattern are characterized by the sinusoidal behavior of Eq. (3), which for a large number of measurements yields the symmetric ρ distribution shown in Fig. 3. Given the random nature of the speckle patterns, previous workers have defined the contrast C on a statistical basis to be the simple ratio of the standard deviation of the intensities σ_I to their expected value $\langle I\rangle^2$. If this is also used to provide a measure of the contrast within the correlation fringe patterns, then the perfect distribution of Fig. 3 yields a contrast value of $C = 0.707$. For comparative purposes, completely random and uniform distributions have contrasts according to this definition of 0.578 and 0, respectively. As a result, the analyses presented below rely heavily on histograms quantitatively characterized by their contrast.

The contrast does not necessarily define the visibility of the fringes, however, as substantial noise remains superimposed on the low spatial frequency fringe patterns as shown in Fig. 2c. Consequently,

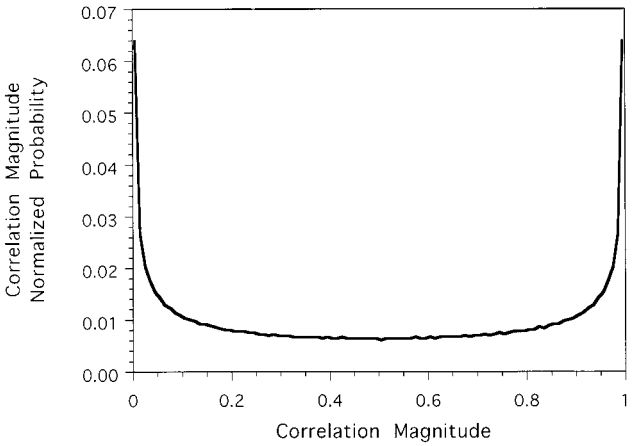

Fig. 3. Expected distribution of correlation amplitudes for perfect noise-free data.

in an ideal correlation fringe pattern, the energy of the low-frequency components should be strongly dominant. An alternative measure is the percentage of the high-frequency noise contained within the correlation fringe pattern image. This is accomplished here by estimating where the bulk of the low-frequency energy lies from the Fourier transform of a hypothetical noise-free forward modeled fringe pattern. This is calculated for the given nominal displacement in the geometrical configuration of the present experiments using Eqs. (3) and (4). All energy at higher frequencies outside of this range is then assumed to be noise, and the integration of this when compared with the integration of the energy over the entire Fourier transform (less any zero frequency component) is taken to be the signal-to-noise ratio.

A series of laboratory tests designed to investigate empirically the conditions under which the direct correlation method will provide the best measurements in light of these limitations on cell size and decorrelation are described below.

3. Experimental Configuration and Speckle Pattern Characterization

The laboratory tests follow a well-known dual-beam illumination design (Fig. 4). Coherent radiation is

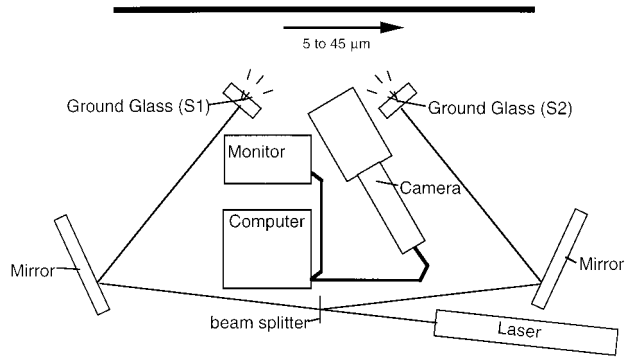

Fig. 4. Experimental geometry.

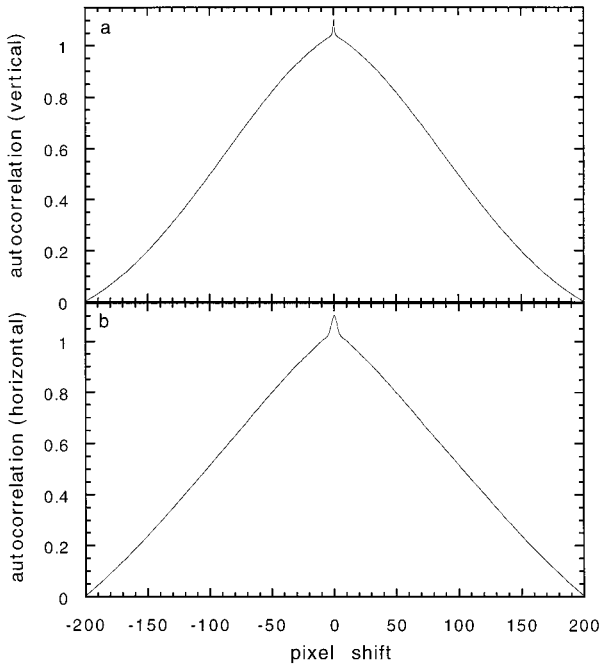

Fig. 5. Details, a, vertically and, b, horizontally through the autocorrelation of Fig. 4a.

supplied by a red 35-mW He–Ne polarized tube laser (Spectra-Physics) with $\lambda = 632.8$ nm. A 50% beam splitter provides two coherent and divergent beams that are each expanded with ground glass (S1 and S2) to illuminate the surface of the object. The object is a flat plate of aluminum (22 cm wide $\times$ 20 cm high) pebbled with a light spray of white paint to improve reflectance, although there is some risk of additional depolarization of the light.[21] The plate is mounted on a translation stage (Klinger, MRL 6.25) controlled with micrometer pistons, which translate the stage to an estimated accuracy of ± 2 μm; as such, the displacement magnitudes reported below in the figures should be considered only as nominal displacements, but the high accuracy of these displacements is not crucial to the present discussion. The tests included

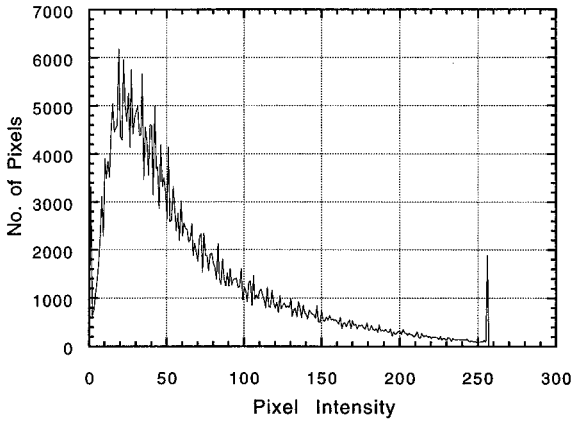

Fig. 6. Histogram of intensities observed in a single raw speckle pattern acquired with the present experimental configuration.

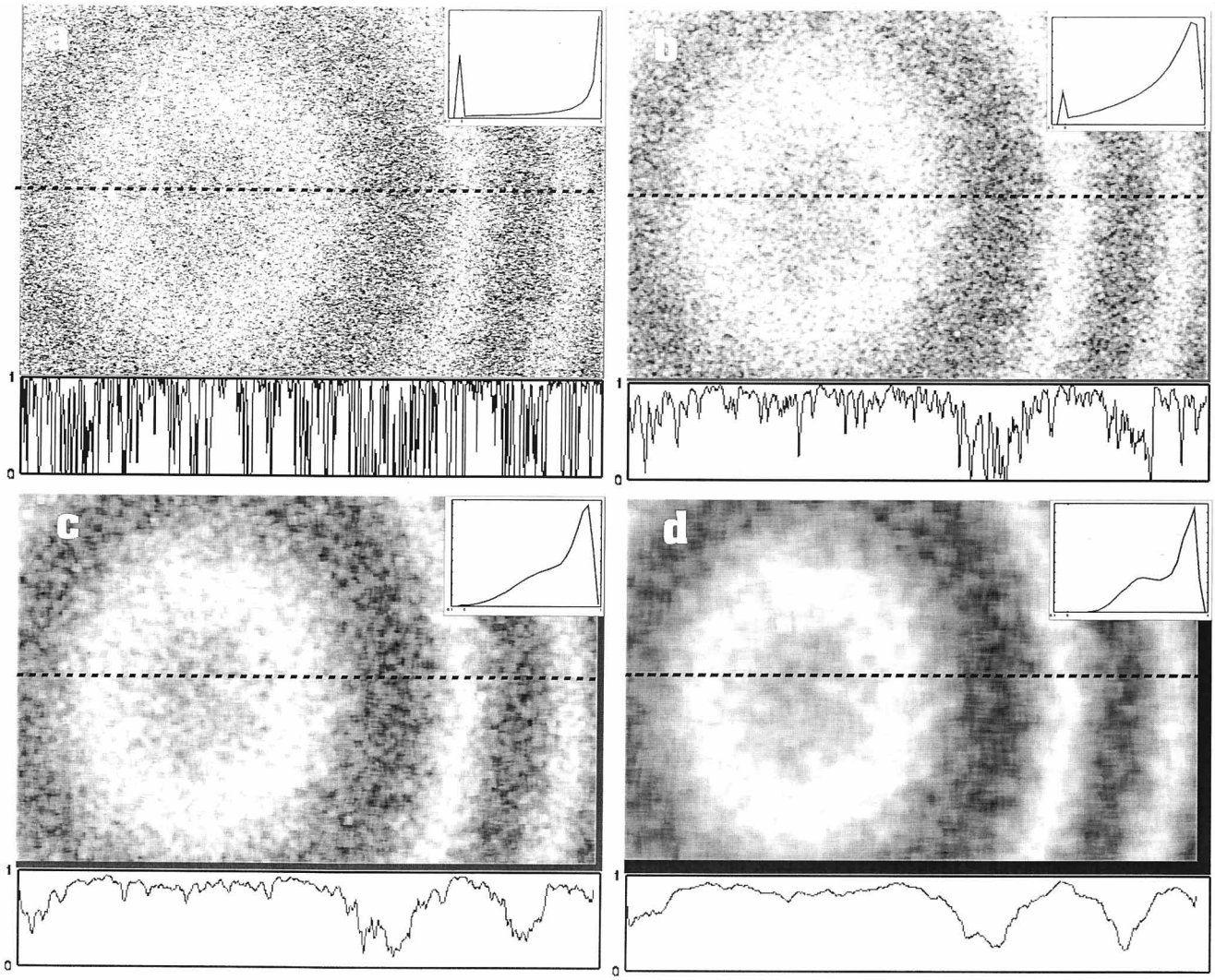

Fig. 7. Correlation fringe patterns for a 10-μm in-plane translation calculated with correlation cells of dimensions, a, 2 × 2; b, 5 × 5; c, 9 × 9; d, 19 × 19. Insets are the corresponding normalized correlation magnitude histograms with independent axes ranging from −0.1 to +1, the range of correlation values for the pixels in the image. Panels beneath each correlation image are the intensities observed along the horizontal profile indicated by the dotted lines through the centers of the images.

a range of in-plane nominal single-axis horizontal translations of the plate toward the right as shown in Fig. 4 with magnitudes ranging from 5 to 45 μm.

A high-resolution gray-scale camera (Sony XC-77) provided images (756 horizontal pixels × 486 vertical pixels), which were digitized with a resolution of 8 bits by an image capture board (Targa+ 16/32). A Canon V6 × 16 − 1.9 (16× magnification), *f* 1.9 irised lens focused the image covering a 6.8-cm × 9.1-cm rectangular region of the plate onto the active area of the CCD device within the camera. Some distortion occurs in the imaging, but on average each pixel corresponds to an area on the plate of 120 μm horizontally and 140 μm vertically, and examples of two typical raw speckle patterns acquired before and after a 30-μm translation have already been given in Fig. 1. This corresponds well to the speckle dimensions of 140 μm as estimated from the autocorrelations of vertical and horizontal profiles through the image and from an estimate of 123 μm based on calculations using the *f*-number and the magnification of the optical system.[21] It is worthwhile to note from sharp portions near the center of the autocorrelations in Fig. 5 that some blurring of the speckles is observed horizontally; the reason for this is unknown, but it probably results from cross-talk between pixels during the horizontal readout scanning of the detector or impedance mismatch problems in the composite video input of the card. The broad curve of the autocorrelation derives from the nonuniform illumination across the initial raw images.

It has long been known and experimentally demonstrated that the intensity distributions for superposed speckle patterns follow an exponential decay.[22] The intensity histogram for a raw speckle pattern acquired with the present experimental arrangement is shown in Fig. 6. Much of this distribution displays the exponential decay save for intensity levels

below 30, which are actually lower than expected. This descrepancy possibly results from the horizontal blurring and also from the fact that the electronic dark current response of the CCD detector had not been removed. Both of these experimental factors would have the effect of shifting the peak of the distribution to slightly higher intensity levels. Alternatively, part of this effect could be the result of partial depolarization of the light by the white-painted surface such that the speckle pattern is not fully developed.[21,22]

4. Results and Discussion

A. Influence of Cell Size

The correlation mappings for a 10-μm in-plane horizontal translation as calculated with a variety of speckle cell dimensions ranging from 2 pixels × 2 pixels to 19 pixels × 19 pixels are shown in Fig. 7. Correlation fringes are visible in each of these images, although the amount of speckle noise appears less with increasing cell dimensions. This is also seen in the intensity profiles for each image; discrimination of individual fringes would be difficult in the single profile for the 2 × 2 cells of Fig. 7a, but this information appears more visible for larger cell dimensions. Clear fringe minima and maxima are seen for the largest of the cell sizes in Fig. 7d but at the expense of some fringe contrast. The profiles all resemble one another, with those acquired from the larger cell dimensions appearing as a low-pass-filtered or smoothed version of the small cell correlation images. Care must be taken, as application of Eq. (5) assumes that the phase does not change substantially over the area of the cell.

In any event, it appears that the crucial information is contained in each of the images of Fig. 7, but various degrees of image processing may be necessary to extract this information. It is difficult to ascertain which cell dimension is best, and this may depend on balancing image quality with calculational speed and the degree of averaging desired. Some insight into the image quality can be gained by examination of the correlation magnitude histograms, the contrast, and measures of the signal-to-noise ratio.

The inset correlation magnitude histograms for each image in Fig. 7 show an evolution with increasing cell dimension with a shape that changes little between Fig. 7c and 7d. Although by straight-eye assessment the fringe quality appears better with increasing cell dimensions, the shape of the histograms diverge from that expected for a perfect fringe pattern in Fig. 3. This mostly results from the averaging inherent in the application of Eq. 5; with increasing cell dimension the minima are shifted upward with fewer and fewer correlation magnitudes near zero.

In Fig. 8, this progressive concentration of the correlation magnitudes under a single peak is seen in the measures of the contrast C defined above. For the 10-μm displacement, this measure of the contrast

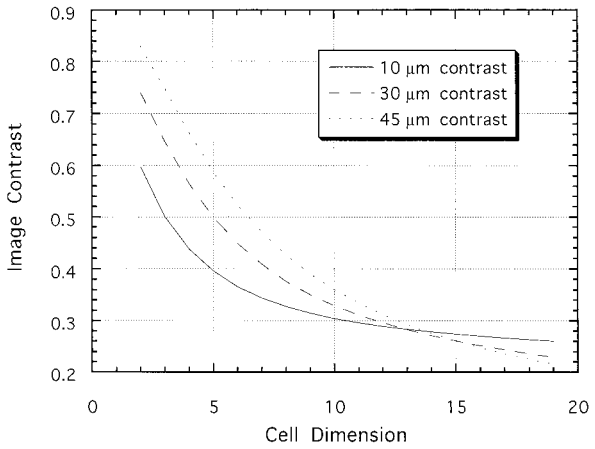

Fig. 8. Contrast as a function of cell dimensions for different displacements.

apparently begins at a high level in apparent agreement with that expected from the histrogram of Fig. 2. However, some care must be exercised in the interpretation as the high-contrast value of Fig. 2 results from the large standard deviation of the dual peaks, whereas for the small cell dimensions in Fig. 7 the more random nature of the correlation magnitudes are responsible.

The signal-to-noise ratio defined above is plotted versus cell dimension for the 10-μm translation in Fig. 9. At small cell dimensions the high-frequency components of the correlation images, providing little useful information on the change in the phase, contain the bulk of the energy. For the 10-μm translation, the useful signal-to-noise ratio is balanced for the 5 × 5 cell (Fig. 7b) and continues to increase for larger cell sizes.

B. Influence of Translation Magnitude

Decorrelation effects result from progressive changes in the speckle pattern owing to slight changes in the geometry of the optical system accompanying motion. Larger motions produce greater decorrelation, which

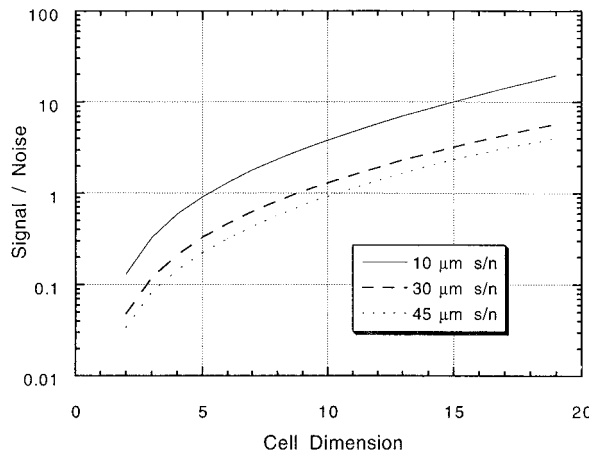

Fig. 9. Signal-to-noise ratio as a function of cell dimension for different displacements.

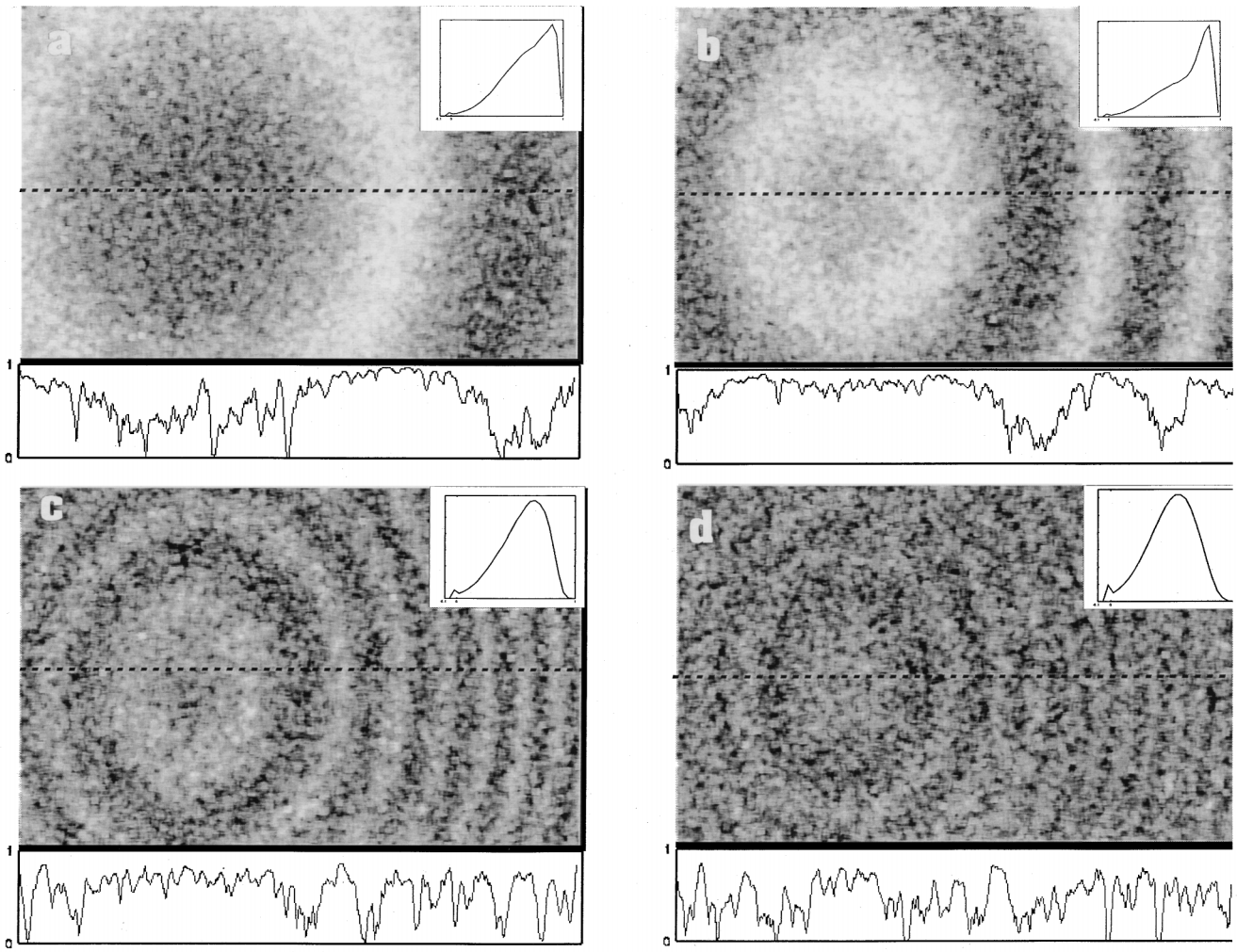

Fig. 10. Correlation fringe patterns calculated with a 9 × 9 correlation cell size for translations of magnitude, a, 5 μm; b, 10 μm; c, 30 μm; d, 45 μm. Insets are the corresponding normalized correlation magnitude histograms with independent axes ranging from −0.1 to +1, the range of correlation values for pixels in the image. Panels beneath each correlation image are the intensities observed along the horizontal profile indicated by the dotted lines through the centers of the images.

results in a degradation of the correlation magnitude images. The critical in-plane translation above which significant decorrelation results is $\Delta x = (\mathrm{NA})\lambda/\mathrm{m}$, where NA is the numerical aperture of the viewing system NA = f/a, where f is the focal length and a is the diameter of the viewing lens aperture.[23] For the present optical system (NA = 14, λ = 632.8 nm, and m = 10.3), the critical translation is ~90 μm, well above the range of the present experiments. Practically, fringe clarity, lost through decorrelation for a given translation magnitude, can be improved by increasing the size of area viewed or by increasing the f-number of the imaging system. However, decorrelation is a progressive feature of the change in the speckle patterns, and for this reason, attempting to evaluate its influence on the image quality is important.

Further, the larger the translation, the more frequent the change of phase across the image and the finer the correlation fringe spacing. Consequently, the larger the translation, the more the phase will vary over the area of a correlation cell with the result that if the correlation cell size is too large, phase information could be lost by an averaging effect.

Examples of correlation magnitude fringe patterns calculated using a constant 19 × 19 cell dimension for in-plane horizontal translations from 5 to 45 μm are shown in Fig. 10 accompanied by magnitude histrograms and profiles as in Fig. 7. Only two dark fringes are seen in Fig. 10a, indicating slightly more than one oscillation in-phase such that the cell size (as indicated by the thickness of the dark band at the bottom and right-hand sides of the image), which is substantially less than the fringe spacing. In contrast, the cell dimensions begin to approach the fringe spacing for the large translation of Fig. 10d with an appreciable decrease in fringe clarity.

The corresponding histograms evolve toward a nearly Gaussian distribution with increasing translation. This results in a progressively lower value of the standard deviation and consequently of the contrast (Fig. 8) for large cell dimensions. In contrast,

the influence of greater decorrelation for the larger translations is seen in the greater values of contrast for small cell dimensions.

The effects of decorrelation on the quality of the images are also seen in the signal-to-noise ratios (Fig. 9). In general, correlation magnitude images contain less relative useful signal with larger translations.

5. Conclusions

A direct correlation method based on the discrete Pearson's coefficient of correlation is used to estimate the local correlation between two speckle patterns acquired before and after translation of an object in an ESPI measurement. The mapping of these calculated magnitudes produces a correlation fringe pattern, and in many respects the present method is similar to the original film-based correlation method.[1] One advantage of the direct correlation is that the illumination over the surface of the object need not be perfectly uniform; the correlation coefficient calculated is automatically normalized over the entire fringe pattern, allowing the method to be used under poor illumination conditions. A second advantage is that the calculation is directly analogous to the theoretically expected local coefficient of correlation and as such by a simple calculation provides the value of the unwrapped phase. A disadvantage of the method is that the calculations to carry out the correlation require more computational effort than is needed for the frame subtraction method.

A series of speckle patterns were acquired with a standard dual-beam ESPI interferometer configuration. The distribution of the speckle intensities observed in a raw pattern generally satisfied the expected exponential decay but was influenced by a horizontal blurring of the speckles and possibly by decorrelation effects associated with the use of the ground glass beam expanders and the white paint coating the surface of the object. This minor shortcoming of the speckle character does not seem to affect the correlation image calculations adversely.

Correlation cell dimensions affect image quality with signal-to-noise ratios progressively increasing with cell dimension. Decorrelation effects intrinsic to the translation also influence the correlation image quality. However, selection of an appropriate criteria for what set of conditions will produce an optimum correlation fringe pattern is not clear. Small cell sizes result in substantial unusable noise within the image but are rapidly calculated. Larger cell dimensions produce less noise in the image but take longer to calculate and also diminish the fringe contrast. Selection of appropriate cell dimensions should be based on the requirements of a given experiment and what further image processing capabilities exist.

Simple square cells were employed in the present study. Research in progress suggests that use of weighted cells with more complex shapes, such as a circular cell with a Gaussian weighting function, will provide better correlation mappings. More complex cell geometry, however, is also accompanied by increased calculation time.

This research was supported by equipment and research grants from the Natural Science and Engineering Research Council of Canada. D. R. Schmitt acknowledges the support of the A. vonHumboldt Foundation during the writing of this paper. Early work was in part supported under an Alberta Oil Sands Technology and Research Authority contract. P. Basran, L. Tober, and J. Haverstock assisted in the setup of the image acquisition system, and C. Schmitt aided in the preparation of the manuscript. We thank the topical editor and a reviewer for their suggested improvements.

References

1. J. A. Leendertz, "Interferometric displacement measurement on scattering surfaces utilizing speckle effect," J. Phys. E Sci. Instrum. **3,** 214–218 (1970).
2. J. C. Dainty, *Laser Speckle and Related Phenomena*, 2nd ed. (Springer-Verlag, Berlin, 1989).
3. R. Jones and C. Wykes, *Holographic and Speckle Interferometry* (Cambridge U. Press, Cambridge, UK, 1983).
4. H. M. Pedersen, "Intensity correlation meterology: a comparative study," Opt. Acta **29,** 105–118 (1982).
5. A. E. Ennos, "Laser interferometry," in *Laser Speckle and Related Phenomena*, 2nd ed., J. C. Dainty, ed. (Springer-Verlag, Berlin, 1989), pp. 203–253.
6. R. Jones and C. Wykes, *Holographic and Speckle Interferometry* (Cambridge U. Press, Cambridge, UK, 1983), Appendix E, p. 333.
7. J. E. Sollid, "Holographic interferometry applied to measurements of small static displacements of diffusely reflecting surfaces," Appl. Opt. **8,** 1587–1595 (1969).
8. E. Archbold, J. M. Burch, and A. E. Ennos, "Recording of in-plane surface displacement by double-exposure speckle photography," Opt. Acta **17,** 883–898 (1970).
9. J. N. Butters and J. A. Leendertz, "A double exposure technique for speckle pattern interferometry," J. Phys. E Sci. Instrum. **4,** 277–279 (1971).
10. K. Biedermann and L. Ek, "A recording and display system for hologram interferometry with low resolution imaging devices," J. Phys. E Sci. Instrum. **8,** 571–576 (1975).
11. O. J. Løkberg and K. Høgmoen, "Vibration phase mapping using electronic speckle pattern interferometry," Appl. Opt. **15,** 2701–2704 (1976).
12. A. J. P. van Haasteren and H. J. Frankena, "Real time displacement measurement using a multicamera phase-stepping speckle interferometer," Appl. Opt. **33,** 4137–4142 (1994).
13. C. Joenthan and B. M. Khorana, "Phase-measuring fiber optic electronic speckle pattern interferometer: phase step calibration and phase drift minimization," Opt. Eng. **31,** 315–321 (1992).
14. S. Johansson and K. G. Predko, "Performance of a phase-shifting speckle interferometer for measuring deformation and vibration," J. Phys. E Sci. Instrum. **22,** 289–292 (1989).
15. J. Kato, I. Yamaguchi, and Q. Ping, "Automatic deformation analysis by a TV speckle interferometer using a laser diode," Appl. Opt. **32,** 77–83 (1993).
16. Z. Jia, "A study of the fracture process in cement-based materials using laser holographic and speckle interferometry," Ph.D. thesis (Northwestern University, Evanston, Ill., 1994).
17. C. Gorecki, "Phase-correlation techniques for quasi real-time measurement of deformations with digital speckle interferometry," Appl. Opt. **33,** 2933–2938 (1994).
18. R. Jones and C. Wykes, "De-correlation effects in speckle-pattern interferometry, 2. displacement dependent de-correlation

and applications to the observation of machine-induced strain," Opt. Acta **24,** 533–550 (1977).
19. X. Peng, H. Y. Diao, Y. L. Zou, and H. Tiziani, "A novel approach to determine decorrelation effect in a dual-beam electronic speckle pattern interferometer," Optik **90,** 129–133 (1992).
20. N. Zhu and F. P. Chang, "Vibration mode shape identification by digital speckle correlation (DISC)," Exp. Tech. **20,** 17–19 (1996).
21. A. E. Ennos, "Laser interferometry," in *Laser Speckle and Related Phenomena*, 2nd ed., J. C. Dainty, ed. (Springer-Verlag, Berlin, 1989), pp. 207–211.
22. J. W. Goodman, "Statistical properties of laser speckle," in *Laser Speckle and Related Phenomena*, 2nd ed., J. C. Dainty, ed. (Springer-Verlag, Berlin, 1989), pp. 21–26.
23. R. Jones and C. Wykes, *Holographic and Speckle Interferometry* (Cambridge U. Press, Cambridge, UK, 1983), pp. 338–339.